Responses of Geomorphic Indices to the Northward Migration of the Eastern Himalayan Syntaxis

Xuemin Pan , Xiaoming Shen * , Zhiyuan He , Xiaoping Yuan , Yukui Ge , Xiong Wu , Yingying Jia , Xiudang Tang

Posted Date: 9 February 2024

doi: 10.20944/preprints202402.0554.v1

Keywords: Eastern Himalayan Syntaxis; geomorphic indices; erosion rates; northward migration

Article

Responses of Geomorphic Indices to the Northward Migration of the Eastern Himalayan Syntaxis

Xuemin Pan [1], Xiaoming Shen [1,*], Zhiyuan He [2], Xiaoping Yuan [3], Yukui Ge [4], Xiong Wu [1,5], Yingying Jia [1] and Xiudang Tang [1]

[1] National Institute of Natural Hazards, Ministry of Emergency Management of China, Beijing 100085, China
[2] Laboratory for Mineralogy and Petrology, Department of Geology, Ghent University, Krijgslaan 281 S8, 9000, Ghent, Belgium
[3] Editorial Department of Earth Science, China University of Geosciences, Wuhan, 430074, Hubei, China
[4] State Key Laboratory of Earthquake Dynamics, Institute of Geology, China Earthquake Administration, Beijing 100029, China
[5] School of Emergency Management Science and Engineering, University of Chinese Academy of Sciences, Beijing 100049, China
* Correspondence: xiaoming_shen@163.com

Abstract: The Eastern Himalayan Syntaxis (EHS), featured by an exceptionally intense compression orogeny and an extremely rapid surface erosion rate, stands out as a prime area for investigating surface processes and landscape evolution. Understanding the formation of the EHS holds significant importance in advancing our comprehension of the evolutionary dynamics within the Tibetan Plateau and the complex interplay between endogenic and exogenic geological processes. Currently, two models, namely the tectonic aneurysm and the syntaxis expansion model, have been proposed to explain the formation and evolution of this syntaxis. In this study, we employ a multi-disciplinary approach, integrating geomorphic indices such as slope, relief, Hypsometric Integral (HI), Normalized Channel Steepness (K_{sn}), River Slope-Basin Area Integration (χ), combined with erosion rates on long-medium-short term timescales obtained from thermochronology, cosmogenic nuclides ^{10}Be and landslide disaster probability data. Our findings suggest a relatively high tectonic activity in the confluence of the Yigong and Parlung Rivers in the northern end of the syntaxis. Moreover, our data reveals that spatial variability of tectonic activity is the primary driver of regional geomorphologic features and the spatial-temporal characteristics of erosion observed in the EHS, with lithology and climatic precipitation playing a lesser role. Furthermore, the northwards migration of the EHS appears to elucidate the shift of tectonic activity and rapid erosion from the core of the syntaxis near the Namche Barwa towards the confluence of the Yigong and Parlung Rivers. This northwards migration of the EHS underscores the need for increased attention to the high geological hazard risk in the northern part of the EHS.

Keywords: Eastern Himalayan Syntaxis; Geomorphic indices; Thermochronology, Cosmogenic nuclides ^{10}Be; Landslide disaster; Dynamic mechanism; Syntaxis expansion.

1. Introduction

The Eastern Himalayan Syntaxis (EHS), stands as a pivotal tectonic occurrence during the Cenozoic, arising from the collision between the Indian and Eurasian plates. Situated within the Himalayan orogenic belt, this region epitomizes robust compression collision and mountain uplift. Its distinctive attributes include intense compression orogeny and a rapid surface erosion rate, rendering it an exemplary natural laboratory and a focal point for investigating collision orogen processes and the intricate interplay between internal and external Earth forcings [1–4]. While

 doi:10.20944/preprints202402.0554.v1

previous researchers have extensively explored this dynamic area, the formation and evolution of the EHS have been the subject of prolong and spirited debate.

At present, models elucidating the development of the EHS fall into two primary categories. One underscores the predominant role of tectonics in the topographic growth, encompassing the duplex thrust or pop-up structure [5] and the "expansion of the syntaxis" model (Figure 1a) [3,6]. The duplex thrust structure involves the folding deformation of the thrust roof occurring in the post-collision phase of the India-Asia collision. This deformation concentrates in the core of the antiform under compressive stress. On the other hand, the pop-up structure posits that the antiform forms first and then migrates northward under extrusion stress, transmitting stress through surrounding fault zones, with deformation mainly concentrated in these zones. The "expansion of the syntaxis" suggests that the early Namche Barwa antiform's deformation was initially constrained by boundary faults, with subsequent northward migration breaking though these constraints [3,7]. In contrast, the alternative perspective emphasizes the preeminence of surface processes in shaping surface morphology, particularly, the "tectonic aneurysm" model (Figure 1b) [8,9]. This model underscores the interconnectedness of tectonic and surface processes, contending that both tectonic uplift centers and rapid erosion centers concentrate in the core area of the Yarlung Zangbo Grand Canyon. Simultaneously, the prolonged and rapid river-driven erosion induces crustal thinning and weaking, triggering mantle upwelling and crustal uplift, further intensifying river-induced surface erosion.

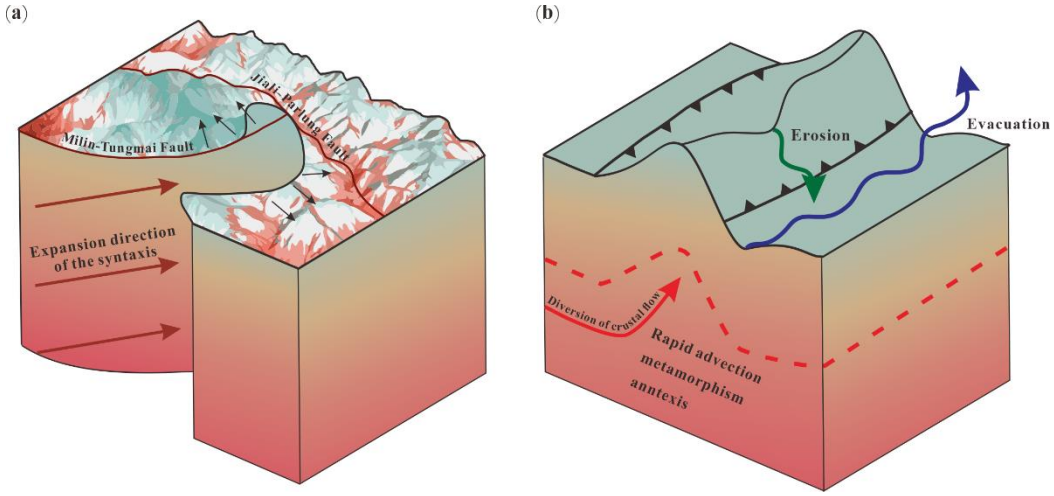

Figure 1. Two main models are proposed for the formation and evolution of the EHS. (**a**) "Expansion of the syntaxis" model [3]; (**b**) "Tectonic aneurysm" model [8].

Most of the research conducted by predecessors has put forth formation and evolution models, along with rapid uplift and exhumation mechanisms for the Namche Barwa region. These models are rooted in various characteristics, such as the interaction between tectonics and erosion [8–10], regional geological features (including magma and rock metamorphism) [11,12], erosion rate, and geochronology and thermochronology [2,13–15]. However, the challenging natural conditions prevalent in the area-covered with snow and vegetation throughout the year-constrain the spatial extent of field geological surveys and sample collection. The geomorphic parameters, sensitive to alterations in tectonic movement, lithology, and climate, serve as effective indicators of geomorphologic evolution and its controlling factors [16,17]. Despite their significance, quantitative analyses of geomorphology in the Namche Barwa region are notably lacking. This gap in research hampers our comprehensive understanding of the evolution of tectonic geomorphology in the region. Given the unique sensitivity of geomorphic parameters to dynamic changes, a more thorough investigation into the quantitative aspects of Namche Barwa's geomorphology is essential for advancing our understanding of the region's tectonic evolution.

In this study, we initiate our investigation by focusing on geomorphic parameters. Leveraging ASTER GDEM v3 30m digital elevation data, we employ the TopoToolbox tool [18] within MATLAB to extract geomorphic indices. This approach, coupled with the integration of thermochronology and

 doi:10.20944/preprints202402.0554.v1

cosmogenic nuclide ^{10}Be, enables us to unveil the spatiotemporal characteristics of rock exhumation/erosion over long-medium-short term time scales. Additionally, our analysis incorporates research on landslide disasters, facilitating a comprehensive exploration of the formation and evolution patterns of the EHS. We delve into the mechanisms governing tectonic activity and erosion, aiming to offer crucial constrains that enhance our understanding of the evolutionary dynamics in the eastern syntaxis.

2. Regional Geomorphology and Geological Background

The EHS is situated in the high mountain canyon region of the southeastern Tibet. It is characterized by a mountainous valley landscape within the eastern Tibetan Plateau, featuring pronounced topographic incisions, including mountains, valleys, and glaciers. The terrain is steep, with overlapping peaks, and the average altitude exceeds 3000 meters. Notably, the eastern Himalayas host two peaks, namely the Namche-Barwa (7782 m) and Gyala-Peri Peaks (7151 m). The rivers in the study area intricately cut through the mountains, forming steep canyon landforms characterized by a large longitudinal slope, turbulent water flow, and significant relative height differences. Both the Yigong and Parlung Rivers sections exhibit canyon landforms with narrow valleys and steep walls, often resembling a "V"-shaped profile. The region's challenging conditions, marked by high river flow rates, potent transportation capacity, and continuous valley deepening, contribute to geological hazards such as landslides and mudslides. The area's climate, primarily influenced by the warm Indian Ocean current and westerly circulation, results in widespread marine glaciers, characterized by humid summers with moderate temperatures and mild, dry winters, creating unique climate conditions.

The eastern syntaxis, formed during the Cenozoic collision between Indian and Eurasian plates, marks the eastern termination of the Himalayan orogenic belt. Its overall configuration reveals a northeast-trending anticline with a northward dipping hup, identified as the Namche Barwa complex anticline. This structure is dissected by surrounding blocks and strike slip faults [5,13]. The strong collision and compression compelled the southward movement of the Indian subcontinent, resulting in a pronounced dislocation and sharp turning of the Indus-Yarlung suture zone to form a distinctive thumb shaped structural knot (Figure 2). The eastern boundary is defined by the Aniqiao-Motuo dextral strike slip fault (AMFS), the western boundary by the Dongjiu-Milin dextral strike slip fault (DMPZ), and the northern boundary comprises a series of northwest-trending faults, including the Jiali-Parlung fault zone (JPFZ), Jiali-Parlung fault zone (JPFZ), the Yarlung-Tsangpo Canyon thrust zone (YTCT), among others [4,5,19–22]. From south to north, the area can be categorized into three rock tectonic units: the Himalayan terrane, India-Yarlung suture zone, and Lhasa terrane [2,24].

 doi:10.20944/preprints202402.0554.v1

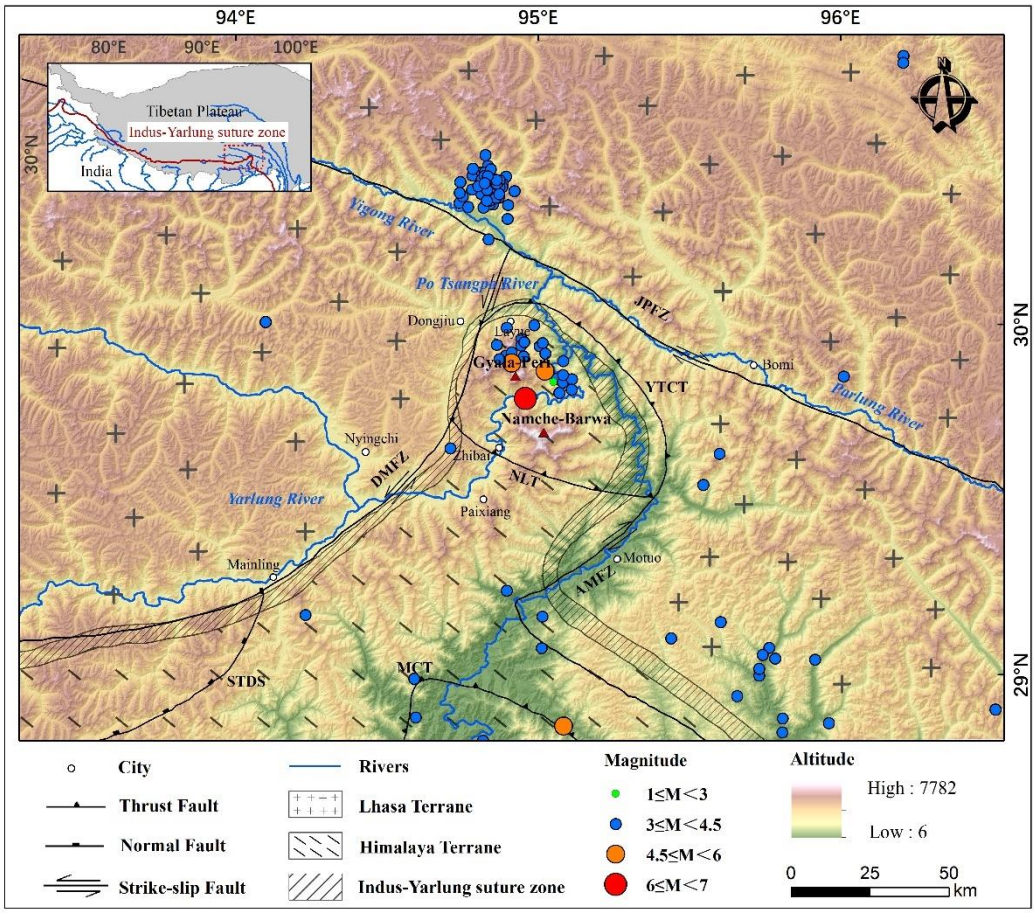

Figure 2. Geologic map of the Namche Barwa syntaxis and nearby region [3,5,9,21,23]. DMPZ: Dongjiu-Milin fault zone; AMFZ: Aniqiao-Motuo fault zone; JPFZ: Jiali-Parlung fault zone; YTCT: Yarlung-Tsangpo Canyon thrust zone; NLT: Namu-La thrust; DEM data are ASTER GDEM v3 with resolution of 30 m, from https://www.gscloud.cn/, accessed on 10 October 2023; earthquake catalog data from https://data.earthquake.cn, accessed on 17 January 2024.

The Himalayan terrane is located on the located on the northern edge of the Indian continent, encompassing the Tethyan Himalayan series and the High Himalayan series. The High Himalayan crystalline rock series, also known as the Namche Barwa Group rocks [24–26], is subdivided into the Duoxiong La, Zhibai, and Paixiang Formations based on original rock formation, metamorphic degree, and metamorphic style, with each group bounded by a ductile shear zone. The Paixiang Formation primarily exposes feldspathic gneiss composed of marble and diopside, with a relatively low degree of metamorphism in the eastern part of the tectonic structure. The Duoxiong La Formation's mixed rock gneiss consists mainly of eyeball-shaped, banded granite gneiss, amphibolite, and a small amount of Precambrian granite intrusions, distributed in the central part of the tectonic nodule. The Zhibai Formation, after experiencing high-pressure granulite facies metamorphism and amphibolite facies retrograde metamorphism, is distributed in a northwest-southeast trend and band within the Paixiang-Zhibai-Gara area of the structural nodules. It contains aluminum-rich felsic gneiss with high-pressure granulite lenses [2,3,5,13,20].

The Lhasa terrane is positioned on the outer side of the EHS. It is distributed in the southern part of the Asian continent and constitutes part of the Eurasian plate [4]. This terrane is mainly composed of the Meso-Neoproterozoic Nyainqentanglha Group metamorphic rock series, Paleozoic magmatic rocks, and the Cretaceous-Paleogene Gangdese magmatic belt. The metamorphic rock series of the Nyainqentanglha Group is concentrated on the eastern side of the Yarlung Zangbo Grand Canyon. It comprises rock combinations of banded migmatite and biotite plagioclase gneiss, featuring locally visible marble, schist, granulite, and plagioclase hornblende. This series has

 doi:10.20944/preprints202402.0554.v1

undergone metamorphism from greenschist to amphibolite, reaching amphibolite and granulite facies. The Cretaceous-period granite rocks represent a series of calcium-alkaline deep-source homologous island arc granite [4,27].

The Yarlung-Tsangpo Canyon thrust zone serves as an ophiolite mélange zone, exposed between the Gangdese magmatic rock zone and the Tethys Himalaya zone. It acts as a divider between the Himalayan terrane and the Lhasa Terrane and is composed of remnants of the new Tethys Ocean crust between the Asian and Indian plates. Ductile shear zones flank both sides of the suture zone, often intersected by radial high-angle brittle strike-slip faults centered on the Namche Barwa peak [27–29]. The ophiolitic mélange predominantly consists of strongly mylonitized ultramafic rocks, mafic rocks, amphibolites, plagioclase amphibolites, muscovite schists, and quartzite. The metamorphic degree ranges from high green schist to low amphibolite facies, mixed with small amounts of marble blocks and foreign rocks from the Nyainqentanglha Group and Namche Barwa Group on both sides [29,30].

3. Materials and Methods

T The DEM data utilized in this study is sourced from the geographic spatial data cloud ASTER GDEM v3 30m resolution digital elevation data (https://www.gscloud.cn/). ASTER GDEM v3 is a global digital elevation model obtained from advanced spaceborne thermal emission and reflection radiometers, based on the observation from NASA's new generation Earth observation satellite Terra. With a global resolution of 30m ASTER GDEM v3 is extensively employed in geomorphological analysis and research, facilitating the extraction of terrain factors and acquisition of geomorphic information. Particularly effective in capturing the basic spatial distribution characteristics of landforms in elevated areas with certain undulations, ASTER GDEM v3 serves as an ideal data source for the geomorphological analysis of the eastern Himalayan tectonic structure. The precipitation data is obtained from the China 1 km resolution monthly precipitation dataset of the National Qinghai Tibet Plateau Science and Technology Data Center (https://data.tpdc.ac.cn/). We collected monthly precipitation data from 2000 to 2022 [31], with a resolution of 1 km and a precipitation unit of 0.1 mm. All data share a common projection (WGS1984_UTM_Zone_47N). Leveraging ArcGIS10.2 and MATLAB TopoToolbox [18] based on DEM data, we extracted rivers and watersheds and calculated river geomorphological parameters. To ensure accuracy in geomorphic parameter calculations, non-bedrock channels (colluvial channels) at the river source were excluded during basin calculations. Finally, a total of 348 rivers were retained along the Yarlung, Yigong, Po Tsangpo, Parlung Rivers and their respective basins.

3.1. Slope and Relief

Slope and terrain undulation are basic geomorphic parameters crucial for characterizing the morphology and evolution of landforms, frequently employed in the quantitative analysis of macroscopic geomorphology [32]. Slope, denoting the degree of ground inclination, is typically represented by the angle between the tangent plane at a specific point on the slope and the horizontal plane. Calculation involves using 3% of DEM data within 3x3 windows derived from the relational class between a given grid point and its surrounding 8 grid points. The slope value signifies terrain flatness, with larger values indicating steeper terrain. Consequently, it serves as an indicator of tectonic geomorphic condition. Beyond a specific slope known as the angle of repose [33], geological disasters like landslides and collapses become more likely, especially when loose accumulation surpasses this critical slope.

Relief measures the difference between the maximum and minimum elevation values in the study area, directly reflecting the relative development level of regional landforms. Young landforms in the early stages of evolution exhibit significant terrain undulation, while older landforms, subjected to prolonged erosion and weathering, show reduced undulation. The calculation formula for terrain undulation is:

$$R = H_{max} - H_{min} \quad (1)$$

 doi:10.20944/preprints202402.0554.v1

In the formula, R is the terrain undulation, H_{max} and H_{min} represents the maximum elevation value and the minimum elevation value, respectively. The terrain undulation has local effects. As the analysis window gradually increases, the undulation continues to increase. However, beyond a certain window size, the increase in undulation slows down. The optimal analysis scale corresponds to the point where the undulation growth stabilizes. The selection of a regional analysis window is critical for accuracy and reflects the macro terrain adequately. Choosing an appropriate analysis window ensures the comprehensive representation of the mountainous body while maintaining universality within a specific area. According to existing research findings [34], the optimum window size for the relief calculation and evaluation in the study area based on the 30 m GDEM is a rectangular neighborhood of 41×41 pixels, equaling to an area of about 1.51 km^2.

3.2. Hypsometric Integral (HI)

The Hypsometric Curve (HC) is a graphical representation employing the relative height ratio of a basin as the vertical axis and the relative area ratio as the horizontal axis. It serves as a geomorphic parameter capturing the residual rate of three-dimensional surface topography volume through a two-dimensional curve. The area elevation integration curve underneath corresponds to the area elevation integration value (HI). A higher HI value signifies a greater residual amount of geomorphic volume within the basin, indicating a reduced level of erosion [35]. The calculation formula is:

$$HI = (E_{meam} - E_{min})/(E_{max} - E_{min}) \quad (2)$$

In equation (2), E_{meam}, E_{min}, E_{max} represent the average altitude, lowest altitude, and highest altitude, respectively. The area elevation integration provides a quantitative reflection of the relationship between geomorphic evolution and tectonic activity. Following Davis's theory of geomorphic erosion cycles, geomorphic evolution is categorized into juvenile, adulthood, and elderly periods, corresponding to HC shapes of convex, S-shaped, and concave, respectively. The evaluation of watershed geomorphology stages and distinctions in erosion dynamics involves constructing functional relationships between area and relative height differences on various contour lines. When HI>0.6, HC typically exhibits an upward convex shape, signifying minimal material erosion in the watershed. During this phase, the watershed displays rough, undulating geomorphic characteristics, indicating the youth stage of evolution. For 0.35 ≤ HI ≤ 0.6, HC generally takes on a 'S' shape, suggesting substantial erosion, maximum terrain undulation, diverse geomorphic types, and complexity—a prime stage in watershed evolution. When HI<0.35, HC typically shows a concave shape, indicating extensive material erosion. At this stage, external dynamic conditions are dominated by accumulation and leveling, resulting in a gradual reduction of terrain undulation. The watershed evolves towards peneplanation, marking the elderly stage of topographic evolution. The area elevation integration is influenced not only by structure, lithology, and climate but is also associated with the choice of basin area and the position of secondary basins within the entire watershed.

3.3. Normalized Channel Steepness(k_{sn})

We use a widely employed model, the stream power erosion model to examine the evolution of river geomorphology. This model delineates the elevation change of the bedrock channel as the difference between the uplift rate (U) of the bedrock and the erosion rate (E) of the river:

$$\frac{dz}{dt} = U(x,t) - E \quad (3)$$

In the formula, z is the elevation of the river channel, x is the distance from the river mouth, and t is the time.

The model expresses the erosion rate E of bedrock rivers as a power function relationship between the river catchment area A and the river gradient S:

$$E = K \cdot A^m \cdot S^n \quad (4)$$

 doi:10.20944/preprints202402.0554.v1

In the formula, K is the river erosion coefficient, influenced by factors like climate, lithology, sediment flux, and river geometry, m is the river catchment area index, and n is the gradient index of the river channel, correlating with the dynamic characteristics of the erosion process, basin hydrological conditions, and the river channel morphology.

When the longitudinal profile of the river attains equilibrium, the bedrock uplift rate and the river erosion rate stabilize, resulting in a steady elevation of the river over time, denoted by $\frac{dz}{dt} = 0$. From equations (3) and (4), it can be concluded that:

$$S = \left(\frac{U}{K}\right)^{\frac{1}{n}} \cdot A^{-\frac{m}{n}} \tag{5}$$

Make $k_s = \left(\frac{U}{K}\right)^{\frac{1}{n}}$、$\theta = \frac{m}{n}$, the quantitative relationship between river gradient S and watershed catchment area A can be expressed by organizing:

$$S = k_s \cdot A^{-\theta} \tag{6}$$

In the formula: k_s represents the steepness index of the river channel, while θ is the concave curvature of the river channel [36], serving as an indicator of the degree of river depression. As the concave index increases, the river channel takes on a more concave shape, resulting in a faster decrease in the elevation of the river channel. Previous studies have determined that a θ value of 0.45 in the Qinghai-Tibetan Plateau region is the most conducive to achieving a balancing channel concavity [36]. Consequently, we utilized this value to compute k_{sn} in our research. Employing the TopoToolbox [18,37], along with 30m resolution DEM data, we employed MATLAB scripts and ArcGIS software for the extraction and computation of k_{sn} across the entire study area.

3.4. River Slope - Basin Area Integration χ (Chi Value)

The χ value, derived from the integration of river slope and watershed area, serve as the area integral along the channel of the bedrock channel incision model [38]. Utilizing the difference in chi values on either side of the watershed provides a measure of watershed stability, offering insights into potential future migration directions [39]. This parameter not only records changes within the watershed but can also signifies river capture events [40,41]. Its versatility is evident in applications ranging from water system restructuring to river capture research [42–44]. Watershed migration is intricately linked to structural, lithological, or climatic shifts. In a stable geomorphic unit, when lithology and climate conditions are uniform on both sides of a mountain, watersheds tend to migrate towards the side experiencing faster uplift. The steep terrain, associated with high erosion rates, leads to watershed migration towards the side with a lower erosion rate — a movement from a low χ value direction to a high χ value direction. However, it is worth noting that some studies indicate that χ value results can be significantly influenced by outlet elevation and lithology, potentially introducing errors in determining watershed migration directions [42]. By simultaneously integrating x on both sides of equation (6), we can acquire:

$$Z = Z(x_0) + \left(\frac{U}{KA_0^m}\right)^{\frac{1}{n}} \chi \tag{7}$$

$$\chi = \int_{x_0}^{x} \left(\frac{A_0}{A}\right)^{\theta} dx \tag{8}$$

The river outlet elevation is represented by $Z(x_0)$, the steepness index by k_s, A_0 is a reference scaling area, and the concave curvature by θ from formulas (7-8), it can be inferred that in a steady state of river, both χ and the elevation of the river channel follow linear first-order functions, commonly expressed as $A_0 = 1m^2$.

4. Results

 doi:10.20944/preprints202402.0554.v1

4.1. Slope and Relief

Figures 3 and 4 illuminate the spatial distribution of slope and relief. These results distinctly capture the structural features of the EHS, revealing a high spatial coherence in the distribution of slope and relief. Notably, the Yigong, Parlung, and Yarlung Rivers, near the core of the syntaxis, exhibit relatively large slope and relief values. Furthermore, the Yigong River basin displays higher slope and relief compared to the Parlung, Po Tsangpo and Yarlung River basins. Elevated slope and relief values are also observed in regions with significant terrain variations, such as Namche Barwa and Gyala Peri Peak. Specifically, high relief values are mainly distributed in the Yigong River, Namche-Barwa Peak, Gala-Peri Peak, and the southeast direction of the syntaxis.

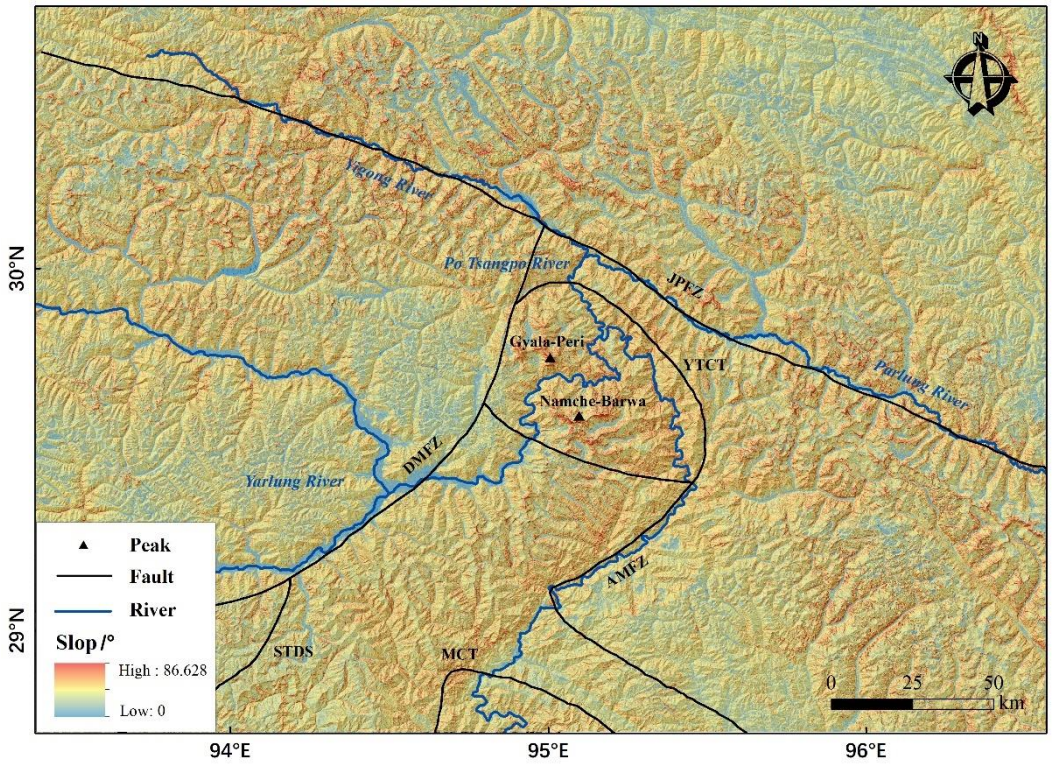

Figure 3. Slope values around the Eastern syntaxis.

 doi:10.20944/preprints202402.0554.v1

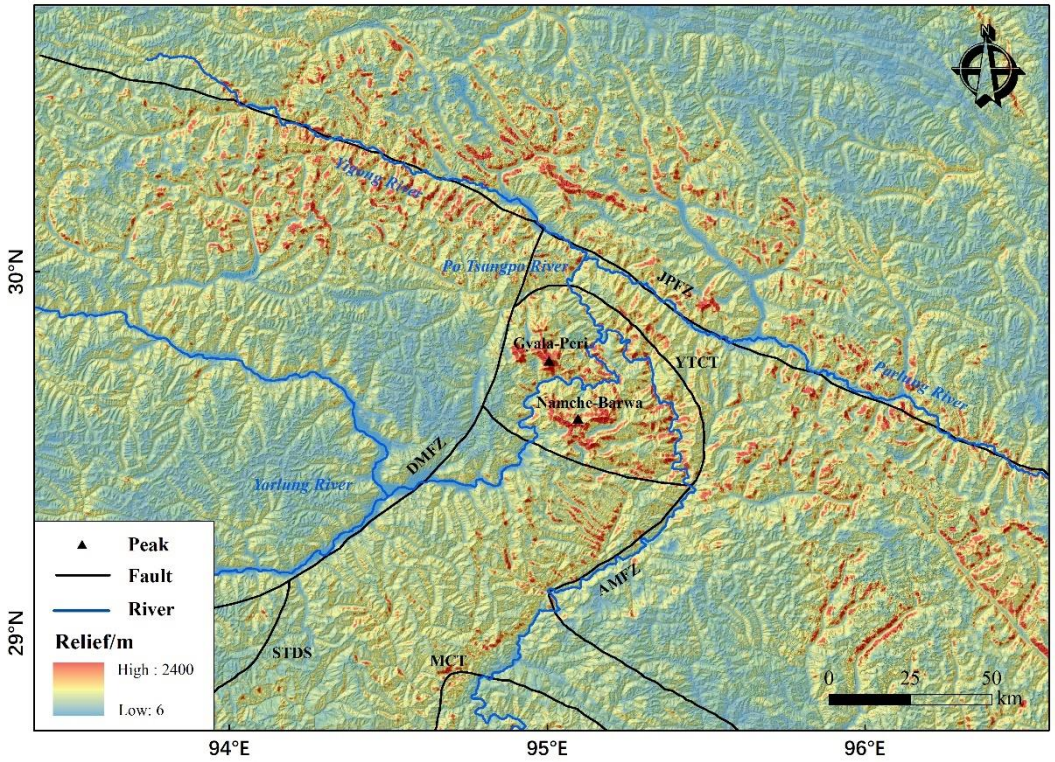

Figure 4. Relief around the Eastern syntaxis.

4.2. Hypsometric Integral (HI)

Figure 5 presents the HI results for 348 bedrock rivers in the Yigong, Parlung, Po Tsangpo, and Yarlung River basins. The HI values for the bedrock channels range from 0.13 to 0.71. Among the 348 watersheds, 324 fall within the HI range of 0.35 to 0.6, indicating a mature stage of geomorphic evolution. This suggests strong erosion in most basin materials within the Eastern syntaxis, resulting in large topographic relief and diverse geomorphic types. Sixteen basins exhibit HI values exceeding 0.6, mainly in the Yarlung River and Po Tsangpo River basins, indicating a youth stage of geomorphic evolution with less erosion. Conversely, eight river basins, primarily in the middle reaches of the Parlung River and a small area in the Yigong River basin, have HI values below 0.35, indicating an old age stage with stable geomorphic forms. It is evident that the HI values in the area around the Namche-Barwa and Gyala-Peri Peak regions do not exhibit significantly high. Notably, the confluence of the three rivers in the northern part of the syntaxis exhibits larger HI values compared to the surrounding watersheds, suggesting a youth and prime stage of watershed evolution with active tectonic activity.

 doi:10.20944/preprints202402.0554.v1

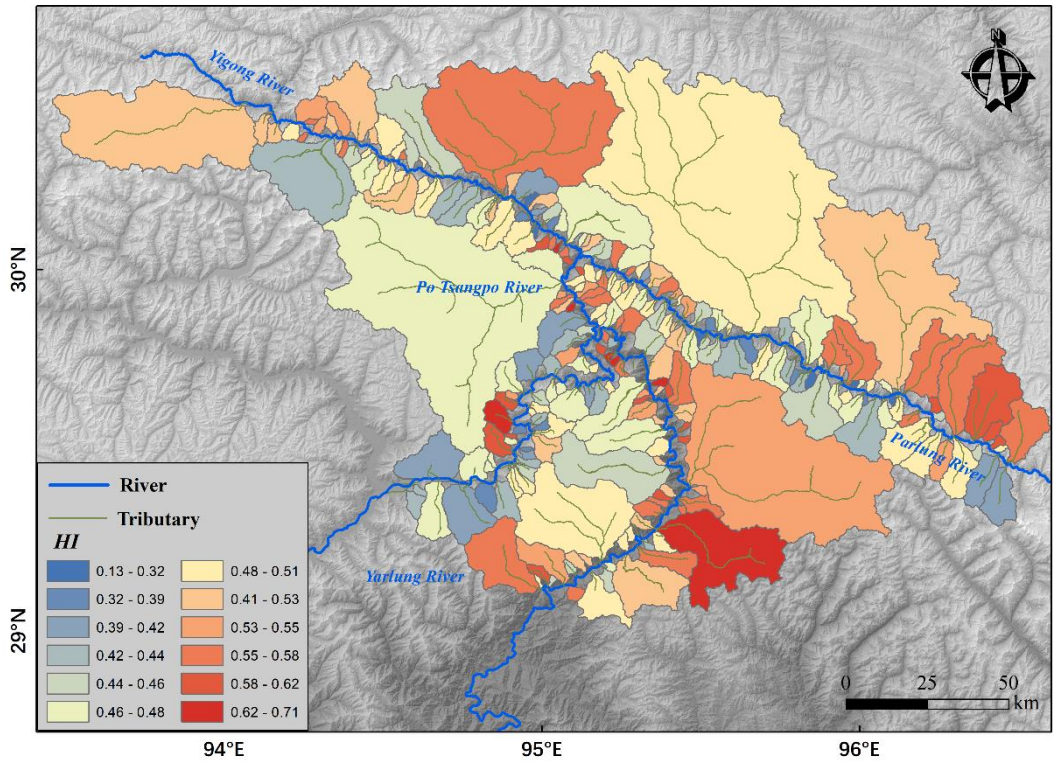

Figure 5. HI values around the Eastern syntaxis.

4.3. Normalized Channel Steepness (K_{sn})

Normalized Channel Steepness (K_{sn}) is calculated for river basins in the EHS bedrock area using the MATLAB platform. Major watersheds, such as the Yigong, Parlung, Po Tsangpo, and Yarlung River basins, show K_{sn} values ranging from 9.67 to 302.84 (Figure 6). The Po Tsangpo River exhibits a notably larger K_{sn} compared to the Yigong, Parlung, and Yarlung Rivers, indicating a steeper topography. The high K_{sn} values are predominantly distributed in the lower reaches of the Parlung and Yigong Rivers, as well as in the Po Tsangpo River and the Great Canyon Region of Yarlung River. This suggests that the core area and northern portion of the EHS Zone display higher K_{sn} values, indicating heightened tectonic activity within this zone. Overall, K_{sn} diffuses outward, decreasing with the Po Tsangpo River basin as the center. Previous studies establish a positive correlation between normalized channel steepness and regional erosion rate [56], indicating an outward diffusion trend and erosion rate reduction centered around the Po Tsangpo River basin.

 doi:10.20944/preprints202402.0554.v1

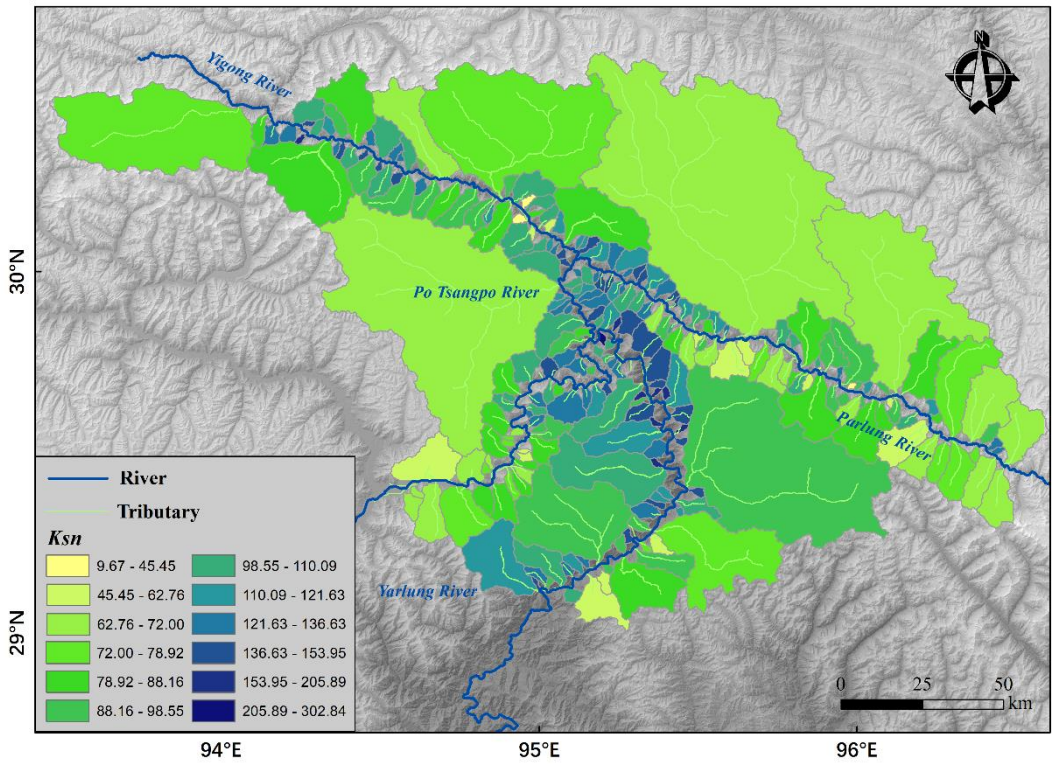

Figure 6. K_{sn} values around the Eastern syntaxis.

4.4. River Slope-Basin Area Integration(χ)

The χ value can reflect watershed migration direction [39]. With a θ value of 0.45 considered suitable for equalizing channel concavity in the Tibetan Plateau region, the distribution map of χ values in the study area is obtained [45]. In this region, we use a constant outlet elevation of 1000m to calculate χ. The southern watershed of the downstream Yigong River displays a tendency to migrate toward the southwest. The southern watershed of the Parlung River, near its convergence with the Yigong River, migrates in a southwesterly direction, while the middle and upper reaches of the Parlung River show a tendency to migrate in the opposite direction. The Yarlung River basin exhibits a southeastward migration trend across the Namche-Barwa peak in the core area of the eastern syntaxis. The Yarlung River basin, away from the syntaxis core, shows a northwestward migration trend.

4.5. Thermochronology-Constrained Long-Term Scale (Million Years) Exhumation Characteristics

Thermochronology has been widely employed to constrain the cooling and exhumation processes of geological structures in various active orogens. The eastern syntaxis, in particular, has been subject to numerous studies by predecessors, resulting in the accumulation of substantial thermochronology data (Figure 7). In this study, five specific dating methods— BtAr (biotite argon) [46], ZFT (zircon fission track) [3], ZHe (zircon helium) [47], AFT (apatite fission track), and AHe (apatite helium)—have been chosen to extract thermochronology data from previous studies [3,7,9,14,48–50]. Using the age2exhume MATLAB program [51], thermal ages were converted into exhumation rates, resulting in a spatial distribution map of the exhumation rates across the study area (Figure 8a). The map reveals distinct spatial features in exhumation rates, with regions exhibiting faster exhumation rates concentrated in the core and northern sectors of the structural junction. Figure 8b illustrates the thermochronological age distribution from the northern part of the syntaxis to its core region, indicating a trend of younger ages in the north and progressively older ages further from the northern sector. The distribution of exhumation rates mirrors the characteristics of the thermochronological age distribution. Figure 8c depicts a discernible decreasing trend in exhumation rates from the northern region of the syntaxis to its core.

 doi:10.20944/preprints202402.0554.v1

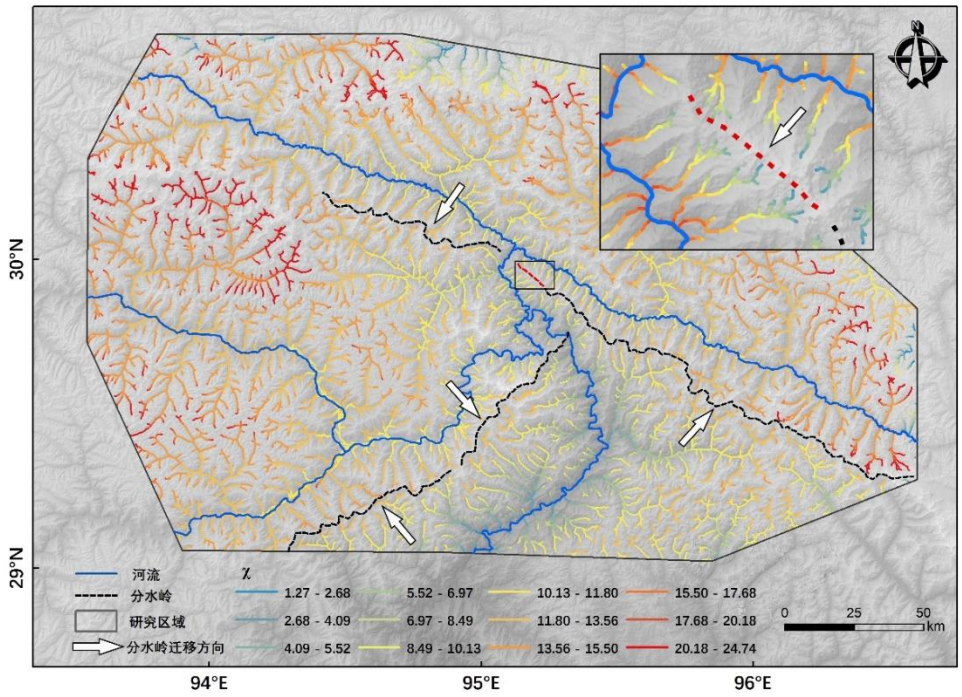

Figure 7. Chi values around the Eastern syntaxis. Dark dashed curve represents the location of divides.

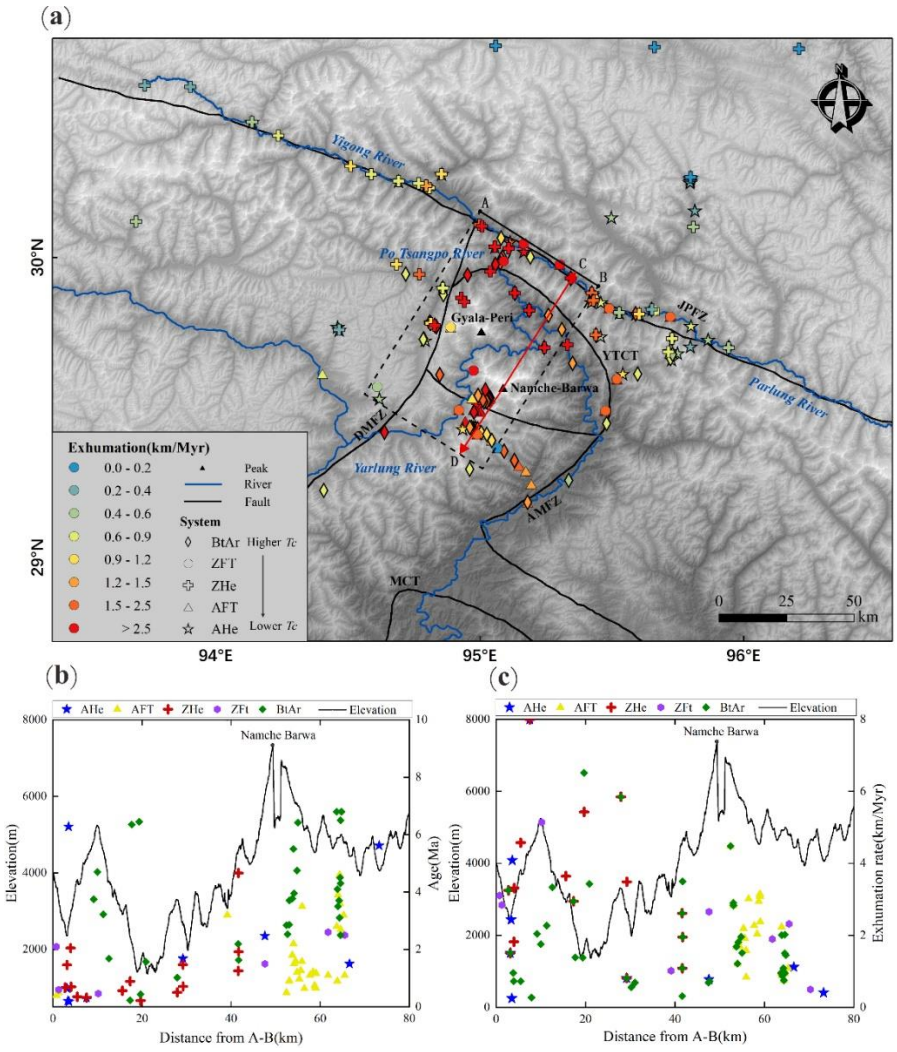

 doi:10.20944/preprints202402.0554.v1

Figure 8. (a) Spatial distribution of previous thermochronometric erosion rate data around the Eastern syntaxis. BtAr (biotite argon), ZFT (zircon fission track), ZHe (zircon helium), AFT (apatite fission track), and AHe (apatite helium)—have been chosen to extract thermochronometric data from previous studies [3,7,9,14,48–50]. ZHe data are from Zeitler et al. (2014) and Yang et al. (2021); ZFt data are from Seward and Burg (2008); BtAr data are from Gong et al. (2008), Zeitler et al. (2014), Gong et al. (2015), and Tu et al. (2015); AHe data are from Zeitler et al. (2014), Yang et al. (2018), and Yang et al. (2021); AFt data are from Lei et al. (2008), Seward and Burg (2008), Yu et al. (2011), and Tu et al. (2015); (b) The graph shows thermochronometric ages from within the black box, distances are calculated perpendicular to the A–B transect. The elevation of line C-D across Namche-Barwa Peak is shown on the left. The highest point of the elevation curve is Namche-Barwa Peak. (c) Same as Figure 8b, except that the coordinates on the right side are replaced by the thermochronometric exhumation rate.

4.6. Cosmogenic Nuclides ^{10}Be-Constrained Medium-Term Scale (Hundred to Ten Thousand Years) Erosion Characteristics

Cosmogenic nuclides serve as a valuable tool for estimating the average erosion rate of river basins over a millennium scale. To gauge the erosion rates at this temporal scale within the eastern syntaxis, we have compiled data on cosmogenic nuclide ^{10}Be erosion rates from previous researchers in the study area [14,52]. This information has enabled us to construct a spatial distribution map illustrating recent erosion rates across the eastern syntaxis (Figure 9a). The ^{10}Be erosion rates in this region span from 0.12 to 4.08 mm/yr. Notably, at the confluence of the Yigong and Parlung Rivers, the erosion rate is relatively high, gradually diminishing towards the upper reaches of both the Yigong and Parlung Rivers. Figure 9b specifically outlines the ^{10}Be erosion rate within the dashed line range south of the straight-line AB in Figure 9a. Here, elevated erosion rates are concentrated in the convergence area of the Yigong and Parlung Rivers in the northern part of the tectonic structure, with rates decreasing progressively southward. The spatial alignment between the ^{10}Be erosion rates and thermochronology-based exhumation rates is striking, signifying a migration of the erosion center from the syntaxis's core area to the convergence region of the Yigong and Parlung Rivers, ultimately pointing towards the northern sector of the syntaxis.

Preprints.org (www.preprints.org) | NOT PEER-REVIEWED | Posted: 9 February 2024 doi:10.20944/preprints202402.0554.v1

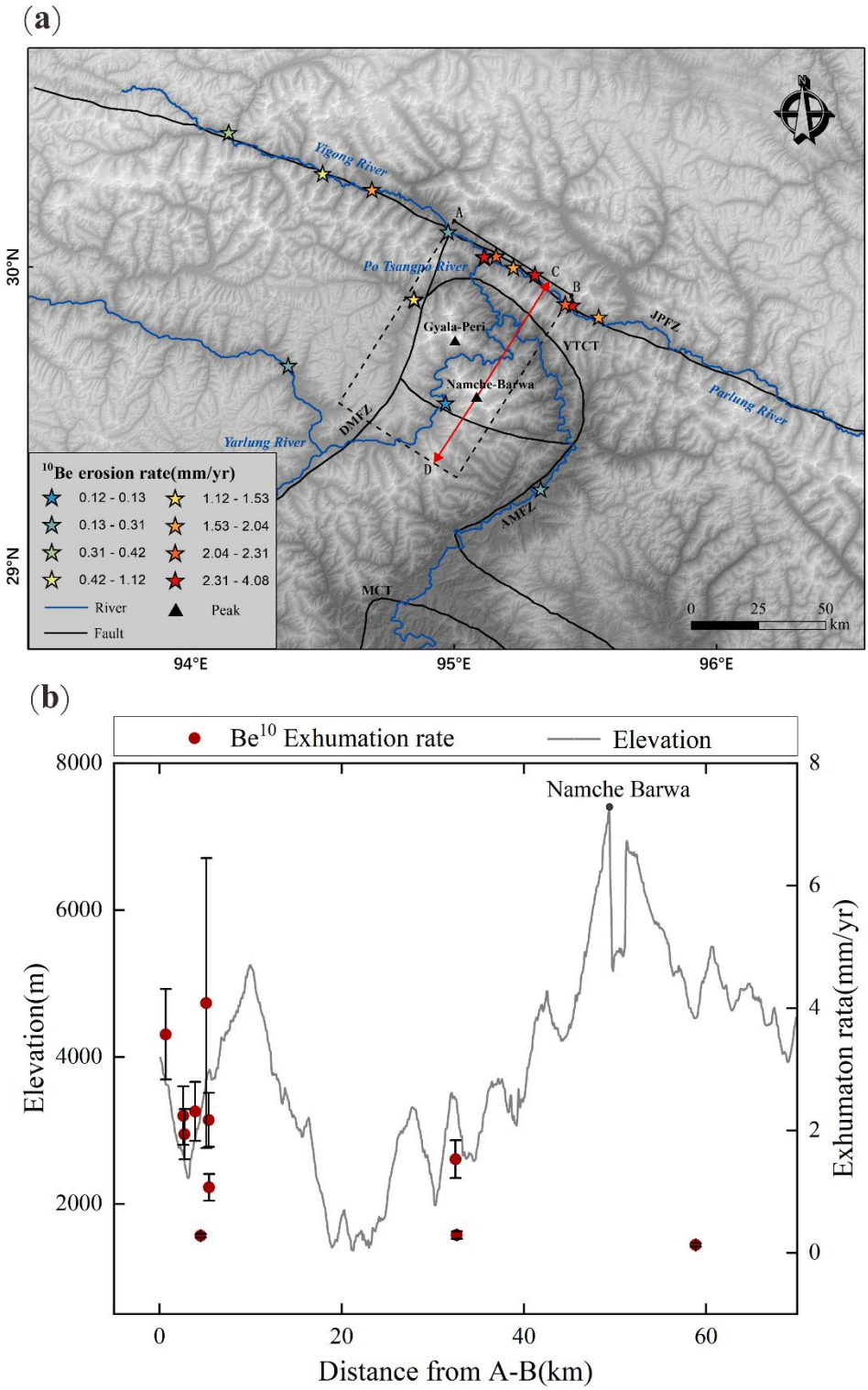

Figure 9. (a) Spatial distribution of previous Cosmogenic nuclides ^{10}Be erosion rate data around the Eastern syntaxis. Previous Cosmogenic nuclides ^{10}Be data are from Evans et al. (2010) and Yang et al. (2021); (b) The graph shows ^{10}Be erosion rate from within the black box, distances are calculated perpendicular to the A–B transect. The elevation of line C-D across Namche-Barwa Peak is shown on the left.

4.7. Landslide Disaster-Constrained Short-Term Scale (Year)

The EHS experienced vigorous regional crustal movements and is characterized by extensive denudation and surface erosion. The geological tectonic environment is notably intricate, marked by a proliferation of active faults. This complex terrain, coupled with intense tectonic activity and

 doi:10.20944/preprints202402.0554.v1

external influences, contributes to frequent geological disasters, including landslide, collapse and debris flow occur frequently in this area. This study also focuses on landslides as a research subject, aiming to investigate the correlation between landslide development characteristics and regional erosion rates. Utilizing the first-generation China earthquake landslide hazard probability map [53], we have generated a spatial distribution map illustrating landslide hazards in the eastern syntaxis (Figure 10).

The spatial distribution of landslide risk predominantly aligns with the Yarlung, Parlung and Yigong Rivers, densely concentrated in regions characterized by rapid denudation. Particularly noteworthy is the high density of landslide hazard development in the Yarlung River's big bend, where erosion is notably robust. The area features narrow valleys, intensifying the downcutting erosion of the rivers. Concurrently, this area is intricately woven and accreted by the suture zone between the Gangdese-Nyainqentanglha domain and the Namche Barwa tectonic wedge terrane, fostering the dense development of landslides within the Yarlung-Zangbo suture zone. Notably, the convergence area of the Yigong and the Parlung Rivers is also an area with a high risk of landslides.

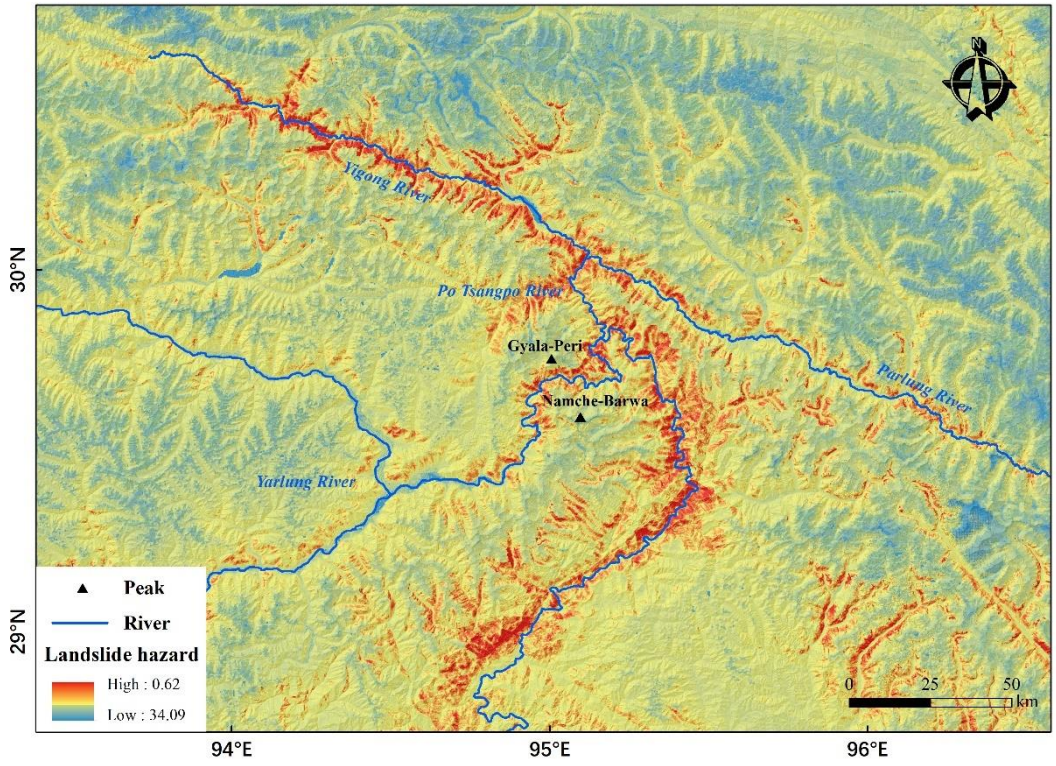

Figure 10. Landslide hazard probability values around the Eastern syntaxis; the landslide hazard probability data are from the Landslide hazard probability first-generation China earthquake landslide hazard probability map [53].

5. Discussion

5.1. Climate and Precipitation

Climate exerts a pivotal influence on geomorphological development, and the eastern syntaxis is distinctly shaped by two contrasting climatic influences. The region to the east of Namche Barwa is under the sway of the Indian Ocean tropical monsoon, originating around 9-6 Ma and extending northward along the Yarlung Zangbo Grand Canyon. Conversely, the region on the west side of Namche-Barwa Peak remains unaffected by the tropical monsoon, retaining a dominant plateau climate due to the hindrance posed by high mountain barriers. The dynamics of water flow significantly contribute to changes in surface morphology through alterations in hydrological conditions and sediment supply within river basins. The regional precipitation conditions largely govern the water system's flow, with river systems predominantly influenced by precipitation.

 doi:10.20944/preprints202402.0554.v1

Discharge, in turn, determines a river's capacity for erosion, transportation, and accumulation, thereby influencing the evolution of topography and geomorphology. Precipitation data for this study were sourced from the monthly precipitation dataset of China, with a resolution of 1km, obtained from the National Tibetan Plateau Data Center (https://data.tpdc.ac.cn/).

We procured month-by-month precipitation data at 1 km resolution for China spanning 2000 to 2022 [31]. Processing this data allowed us to derive the spatial distribution of mean annual precipitation in the study area for the same period (Figure 11). The average annual precipitation in the study area ranges from 33.87 to 186.54 mm, exhibiting a decreasing trend from southeast to northwest. The most noticeable disparities are observed on the southeast and northwest sides of Gyala-Peri and Namche-Barwa Peaks, with precipitation showing no significant variation on both sides of the Yigong River. Interestingly, we observed that the precipitation-prone area did not completely align with the landslide geohazard-prone area, and geomorphologic parameters exhibited significant changes. This decoupling phenomenon suggests that precipitation does not wield a substantial control effect on geomorphic indices in the eastern syntaxis area.

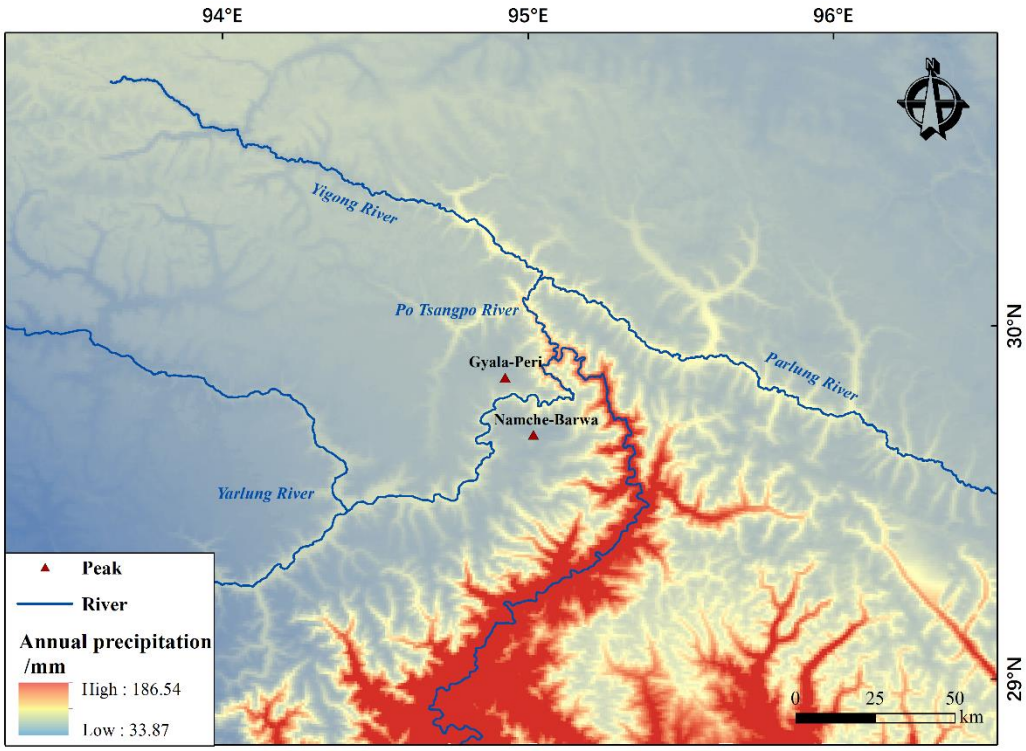

Figure 11. Mean annual precipitation data around eastern syntaxis from 2000 to 2022; the precipitation data are from https://data.tpdc.ac.cn, accessed on 7 November 2023.

5.2. Lithology

Lithology plays a crucial role in shaping geomorphic evolution, as it directly influences the surface's resistance to erosion. By altering the erosional resistance of the surface, lithology significantly impacts geomorphic development and subsequently shapes surface morphology.

The Proterozoic, Carboniferous-Permian, and Jurassic strata are extensively distributed throughout the study area (Figure 12). The Proterozoic strata are predominantly exposed in the core region of the EHS, encompassing the Yarlung River Basin, Po Tsangpo River Basin, and southern side of the Parlung River Basin. These exposed lithologies comprise gneiss, marble, quartzite, and slate, exhibiting remarkable resistance to erosion. The Carboniferous-Permian strata are mainly distributed in the Yigong River basin and the northern side of the lower reaches of the Parlung River, comprising sandstone, slate, and conglomerate with relatively low resistance to erosion. The Jurassic strata are primarily distributed in the northern region of the Yigong River and the Parlung River, exhibiting outcropping rock formations composed of granite, diorite, and porphyry that possess relatively high

 doi:10.20944/preprints202402.0554.v1

resistance to erosion. In addition to the above widely distributed strata, numerous smaller outcropping strata in the study area, with various rock types and lithologies. Different types of rocks exhibit varying degrees of erosion resistance, thereby exerting a significant influence on the regional geomorphic evolution. Comprehensive lithologic analysis shows that the erosion resistance of the bedrock in the southern side of the Parlung River is higher than that in the northern side. Despite not taking into account rainfall and tectonic factors, it would be expected for the HI and Ksn values to be higher on the southern side compared to those on the northern side; however, empirical findings do not demonstrate a significant disparity. The geomorphic indices in the study area are not greatly affected by lithology. Similarly, this phenomenon is also observed in other locations within the study area, indicating that lithology exerts a relatively negligible influence on river geomorphic indicators in the EHS.

Altogether, the rock types in the EHS exhibit a high degree of complexity and varying degrees of erosion resistance. However, despite changes in lithology at the syntaxis, there are no significant differences observed in geomorphic parameters in different lithologic areas. Therefore, it can be inferred that the lithology of the EHS area exerts minimal influence on geomorphic evolution.

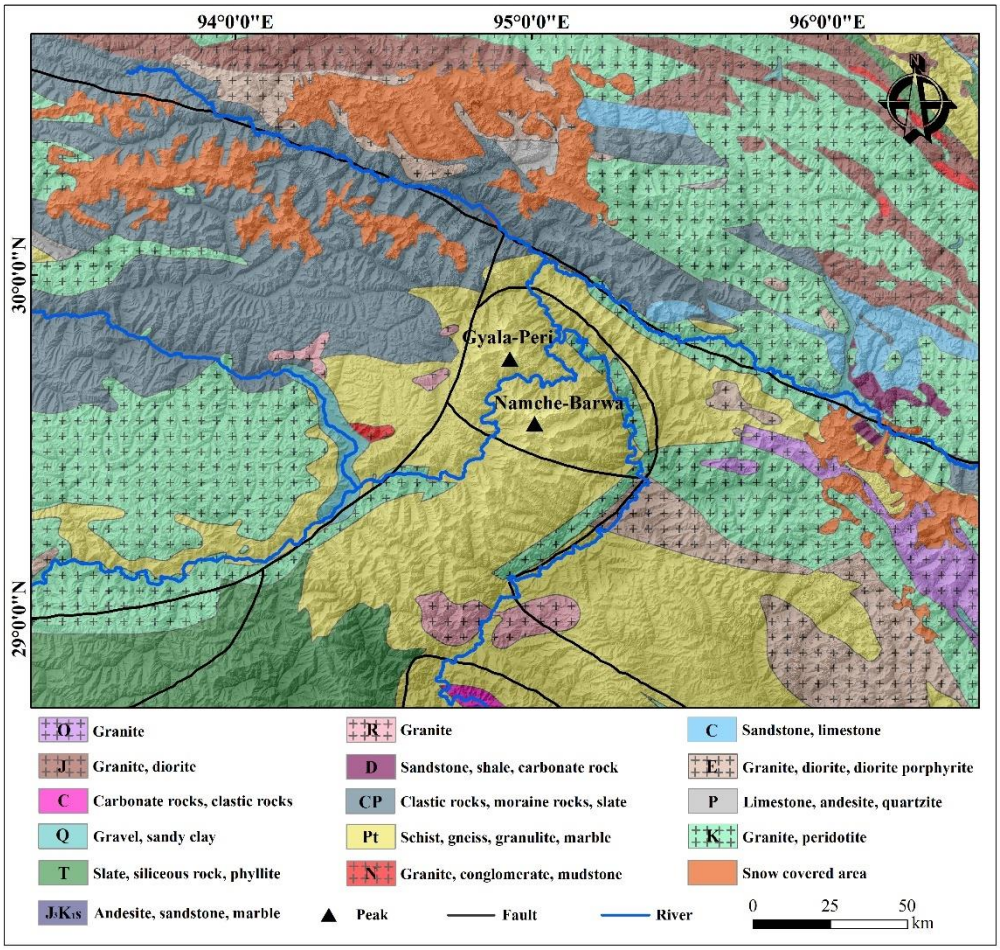

Figure 12. Lithology around the Eastern syntaxis; the regional lithologic data are from the https://www.ngac.org.cn, accessed on 25 November 2023. (O: Ordovician; J: Jurassic; Є: Cambrian; Q: Quaternary; T: Triassic; J_3K_{1S}: Upper Jurassic Lower Cretaceous; R: Tertiary; D: Devonian; CP: Carboniferous Permian; Pt: Proterozoic; N: Neogene; C: Carboniferous; E: Paleogene; P: Permian; K: Cretaceous period; The cross symbol is granite;).

5.3. Tectonics

Our geomorphic analysis highlights a correlation between geomorphic indices and tectonic activity, revealing active tectonic activity in the area where the Yigong and Parlung Rivers converge

 doi:10.20944/preprints202402.0554.v1

in the northern part of the syntaxis (Figures 5 and 6). However, our results indicate a weak correlation between tectonic activity and slope, as well as topographic relief. This weak correlation observed in our study is not consistent across all geomorphic indices, such as HI, K_{sn}, χ, in particular, can quantitatively reflect the relationship between geomorphic evolution and tectonic activity. In the convergence area of the Yigong and Parlung Rivers in the northern part of the syntaxis, HI exhibits a significantly high value, indicating active tectonic activity in the region accompanied by rapid erosion. In the Po Tsangpo River basin, the river channel steepness index, K_{sn}, has a notably high value, suggesting that the terrain in this area is steep, leading to faster erosion compared to other regions of the syntaxis. The K_{sn} has been proposed as a good predictor for erosion rates, and shows a positive correlation with erosion rate [54], suggesting active tectonic activity and rapid erosion in the northern part of the syntaxis. Additionally, the Chi value serves as a reflection of the migration direction of the watershed (Figure 7). In the northern part of the syntaxis, the watershed to the south of the Yigong River demonstrates a southward migration trend. Goren et al. [55] noted that the watershed tends to migrate towards areas with a low erosion rate, further emphasizing the higher erosion rate in the northern syntaxis.

For a long timescale, our collection of thermochronological data provides insights into erosion rates (Figure 8). Analyzing the spatial distribution of erosion rate data derived from thermochronological ages reveals that the rapid erosion center in the eastern syntaxis extends beyond the core area of Namche Barwa to the convergence area of the Yigong and Parlung Rivers in the northern syntaxis. Similarly, at a short-term scale, erosion rates represented by the cosmogenic nuclide ^{10}Be show consistent results (Figure 9).

Examining the spatial distribution map of landslide risk on a short timescale (Figure 10), high-risk values are observed in the core and northern areas of the syntaxis. The distribution of erosion features differs from that on long and short period scales (Figures 8 and 9), particularly in the Yigong and Yarlung River basins. The heightened landslide risk in the downstream of the big bend of the Yarlung River correlates with the substantial precipitation in this area (Figure 11), highlighting precipitation as the primary factor causing landslides in this region. Conversely, in the Yigong River basin, where higher landslide risk is not associated with low precipitation or significant lithological influence, we attribute the dominant cause of landslides to tectonic factors.

In summary, the confluence area of the Parlung River and the Yigong River is tectonically highly active over at least the past 2 Myr based on the geomorphic indices (e.g., HI and Ksn) and erosion characteristics at different time scales. This conclusion is supported by lines of geological evidences. Enhanced Quaternary uplift in the lower reaches of the Yigong and Parlung Rivers in the northern boundary of the syntaxis was revealed by thermochronometric and cosmogenic nuclide studies [23,56–58]. Capture of the Yigong River by the Yarlung Tsangpo River was possibly occurred in the late Quaternary derived by the provenance analysis of sediments in the distal foreland basin [59], thermoluminescence thermochronometry and analysis of the morphology of the Yigong River profile [23]. This capture event has also been attributed to intense tectonic activity to the immediate north of the syntaxis in the recent geological past [6,23].

5.4. Dynamic Mechanism and Its Implications for Geological Hazard

The prevailing controversial models regarding the rapid uplift mechanism in the EHS center on the ‘tectonic aneurysm’ model [8,9] and the ‘expansion of the syntaxis’ model [3,6]. These models differ significantly in terms of the evolution pattern of the water system and the spatial variation pattern of surface erosion rates. According to the ‘tectonic aneurysm’ model, the river knickpoint results from the long-term coupling of river tectonic uplift and erosion, remaining stable over time. Conversely, the ‘expansion of the syntaxis’ model proposes an unstable river knickpoint that migrates due to the deformation and drag of the river system [3]. The spatial pattern of erosion rates has been proposed to distinguish these models, with the ‘tectonic aneurysm’ model concentrating the rapid erosion center consistently in the Yarlung Zangbo Grand Canyon region. In contrast, the ‘expansion of the syntaxis’ model suggests that the rapid erosion center will migrate with the expansion direction of the anticline. This study focuses on discerning the spatial variation pattern of geomorphic indices

 doi:10.20944/preprints202402.0554.v1

and rapid erosion centers, making the tectonic activity and erosion rate patterns of the EHS the key factors in distinguishing between these two models.

The spatial distribution of tectonic activity and erosion rates across long to short timescales, assessed through comprehensive geomorphological analysis, thermochronology, cosmogenic nuclides, and landslide disaster probability, collectively indicates the expansion of the rock uplift and rapid erosion center to the convergence area of the Yigong and Parlung Rivers in the northern syntaxis. This aligns with the concept proposed by the expansion of the syntaxis model, suggesting the migration of the rock uplift and rapid erosion center with the direction of anticline expansion [3,6,7]. As suggested by King et al. (2016), the confluence area of the Yigong and Parlung Rivers coincides with the main axial plane of the Namche Barwa antiform, and therefore a northward expansion of the antiform along this plane would have resulted in enhanced rock uplift and erosion. This northward migration of the syntaxis aligns with a series of proposed mechanical models [60–62] and the main shortening direction observed in geodetic data [63]. Recently, Yang et al. (2021) reconstructed the path of the northward migration of the syntaxis over the past 6 Myr by inversion modeling of regional thermochronological ages. Furthermore, spatial distribution differences between the precipitation and denudation data (Figures 8, 10 and 11) underscore the decoupling between tectonics and surface processes in this region, contradicting the erosion pattern described by the 'tectonic aneurysm' model.

Our new geomorphic analysis results, combined with the observations mentioned above, suggest that the high tectonic activity in the northern end of the syntaxis is probably induced by the northward migration of the syntaxis. This has significant implications for the evaluation and prediction of the geological hazards. Geological hazards such as landslide, debris flow and earthquake are tightly related to tectonic activity. The steep topography, high erosion rate and intense rock uplift make the northern part of the EHS having a high risk of geological hazards, although there has never been a major earthquake in this area (Figure 2).

6. Conclusions

We leverage ASTER GDEM V3 30m digital elevation data and employ the ArcGIS and TopoToolbox tool within MATLAB to extract several geomorphic indices. This approach is coupled with the integration of thermochronology, cosmogenic nuclide ^{10}Be and landslide hazard probability data. We delve into the mechanisms governing tectonic activity and erosion, offering crucial constraints on the evolutionary dynamics in the eastern syntaxis. The results of the study are as follows:

(1) Our comprehensive geomorphic analysis highlights a correlation between geomorphic indices and tectonic activity, revealing relatively high tectonic activity in the area where the Yigong and Parlung Rivers converge in the northern part of the syntaxis. The spatial difference in geomorphic index values reflects the variability of tectonic activity, and suggests a relatively minor impact of lithology and climatic precipitation.

(2) The high tectonic activity in the convergence area of the Yigong and Parlung Rivers revealed by geomorphological analysis, is supported by the spatial consistent distribution of erosion rates across long to short timescales, assessed through thermochronology, cosmogenic nuclides and landslide disaster probability. Combined previous geological observations and modeling results, we suggest that the active center of the EHS has migrated from the core near the Namche Barwa to the northern end of the syntaxis.

(3) We propose that both the tectonic activity and spatiotemporal characteristics of rock erosion were consequences of the northward expansion of the syntaxis, indicating the dominating role of tectonic deformation in driving the geomorphic evolution of the syntaxis. The high risk of geological disasters in the northern part of the EHS deserves great attention.

Author Contributions: Conceptualization, X. S.; Data curation, X. P. and X. S.; Formal analysis, X. P., X. S. and Z. H.; Funding acquisition, X. S.; Investigation, X. P., X. S., Z. H., Y. G., Y. J. and X. T.; Methodology, X. P., X. S., Z. H., X. Y., Y. G., X. W. and X. T.; Project administration, X. S.; Resources, X. S.; Software, X. P., X. S., X. W. and

Y. J.; Supervision, X. S.; Validation, X. P., X. S., Z. H., X. Y. and Y. J.; Visualization, X. S.; Writing – original draft, X. P.; Writing – review & editing, X. S., Z. H. and X. Y.

Funding: This research was funded by the National Natural Science Foundation of China (42073052) and the National Key Research and Development Program of China (Grant No. 2022YFF0800903).

Data Availability Statement: We The geographic spatial data cloud ASTER GDEM v3 30m resolution digital elevation data are from the website (https://www.gscloud.cn, accessed on 10 October 2023). The earthquake catalog data are from the website (https://data.earthquake.cn, accessed on 17 January 2024). The precipitation data are from the website (https://data.tpdc.ac.cn, accessed on 7 November 2023). The regional lithologic data are from the website (https://www.ngac.org.cn, accessed on 25 November 2023).

Acknowledgments: We thank Chong Xu for providing the data of landslide hazard probability.

Conflicts of Interest: The authors declare no conflict of interest.

References

1. Beaumont, C.; Jamieson, R.A.; Nguyen, M.; Lee, B. Himalayan tectonics explained by extrusion of a low-viscosity crustal channel coupled to focused surface denudation. Nature **2001**, 414, 738-742.
2. Booth, A.L.; Zeitler, P.K.; Kidd, W.S.; Wooden, J.; Liu, Y.; Idleman, B.; Hren, M.; Chamberlain, C.P. U-Pb zircon constraints on the tectonic evolution of southeastern Tibet, Namche Barwa area. American Journal of Science **2004**, 304, 889-929.
3. Seward, D.; Burg, J.-P. Growth of the Namche Barwa Syntaxis and associated evolution of the Tsangpo Gorge: Constraints from structural and thermochronological data. Tectonophysics **2008**, 451, 282-289.
4. Xu, Z.Q.; Cai, Z.H.; Zhang, Z.M.; Li, H.Q.; Tang, Z.M. Tectonics and fabric kinematics of the Namche Barwa terrane, Eastern Himalayan Syntaxis. Acta Petrologica Sinica **2008**, 24, 1463-1476.
5. Ding, L.; Zhong, D.; Yin, A.; Kapp, P.; Harrison, T.M. Cenozoic structural and metamorphic evolution of the eastern Himalayan syntaxis (Namche Barwa). Earth and Planetary Science Letters **2001**, 192, 423-438.
6. King, G.E.; Herman, F.; Guralnik, B. Northward migration of the eastern Himalayan syntaxis revealed by OSL thermochronometry. Science **2016**, 353, 800-804.
7. Yang, R. Exhumation and topographic evolution of the Namche Barwa Syntaxis, eastern Himalaya. Tectonophysics **2018**, 722, 43-52.
8. Zeitler, P.K.; Meltzer, A.S.; Koons, P.O.; Craw, D.; Hallet, B.; Chamberlain, C.P.; Kidd, W.S.; Park, S.K.; Seeber, L.; Bishop, M. Erosion, Himalayan geodynamics, and the geomorphology of metamorphism. Gsa Today **2001**, 11, 4-9.
9. Zeitler, P.K.; Meltzer, A.S.; Brown, L.; Kidd, W.S.; Lim, C.; Enkelmann, E. Tectonics and topographic evolution of Namche Barwa and the easternmost Lhasa block, Tibet. In Toward an improved understanding of uplift mechanisms and the elevation history of the Tibetan Plateau; Geological Society of America Special Papers: **2014**; Volume 507, pp. 23-58.
10. Koons, P.O.; Zeitler, P.; Hallet, B. Tectonic aneurysms and mountain building. Treatise on geomorphology **2013**, 5, 318-349.
11. Bracciali, L.; Parrish, R.R.; Najman, Y.; Smye, A.; Carter, A.; Wijbrans, J.R. Plio-Pleistocene exhumation of the eastern Himalayan syntaxis and its domal 'pop-up'. Earth-Science Reviews **2016**, 160, 350-385.
12. Sun, Z. M.; Zheng, L. L.; Geng, Q. R. Genetic mechanisms and exhumation processes of the high-pressure granulites within the Eastern Himalayan syntaxis, Xizang. Sedimentary Geology and Tethyan Geology **2004**, 24, 22-29.
13. Burg, J.-P.; Nievergelt, P.; Oberli, F.; Seward, D.; Davy, P.; Maurin, J.-C.; Diao, Z.; Meier, M. The Namche Barwa syntaxis: evidence for exhumation related to compressional crustal folding. Journal of Asian Earth Sciences **1998**, 16, 239-252.
14. Yang, R.; Herman, F.; Liu, T.; Biswas, R.H.; Fellin, M.G.; Tian, Y.; Gong, J.; Jiao, R.; Maden, C.; Chen, H. Enhanced Quaternary exhumation in the Namche Barwa syntaxis, eastern Himalaya. Geology **2021**, 49, 958-962.
15. Lei, Y.; Zhong, D.; Ji, J.; Jia, C.; Zhang, J. Fission track evidence for two Pleistocene uplift-exhumation events in the Eastern Himalayan syntaxis. Quaternary Sciences **2008**, 28, 584-590.
16. Owen, L.A. Tectonic geomorphology. International Encyclopedia of Geography: People, the Earth, Environment and Technology: People, the Earth, Environment and Technology **2016**, 1-9.
17. Yeats, R.; Sieh, K.; Allen, C. Geology of earthquakes: Oxford University Press. New York **1997**, 568.

18. Schwanghart, W.; Kuhn, N.J. TopoToolbox: A set of Matlab functions for topographic analysis. Environmental Modelling & Software **2010**, 25, 770-781.
19. Deng, Q.; Zhang, P.; Ran, Y.; Yang, X.; Min, W.; Chu, Q. Basic characteristics of active tectonics of China. Science in China Series D: Earth Sciences **2003**, 46, 356-372.
20. Liu, Y.; Zhong, D. Petrology of high-pressure granulites from the eastern Himalayan syntaxis. Journal of Metamorphic Geology **1997**, 15, 451-466.
21. Xu, Z.; Ji, S.; Cai, Z.; Zeng, L.; Geng, Q.; Cao, H. Kinematics and dynamics of the Namche Barwa Syntaxis, eastern Himalaya: Constraints from deformation, fabrics and geochronology. Gondwana Research **2012**, 21, 19-36.
22. Zhang, J.; Ji, J.; Zhong, D.; Ding, L.; He, S. Structural pattern of eastern Himalayan syntaxis in Namjagbarwa and its formation process. Science in China Series D: Earth Sciences **2004**, 47, 138-150.
23. Yang, R.; Herman, F.; Liu, T.; Biswas, R.H.; Fellin, M.G.; Tian, Y.; Gong, J.; Jiao, R.; Maden, C.; Chen, H. Enhanced Quaternary exhumation in the Namche Barwa syntaxis, eastern Himalaya. Geology **2021**, 49(8), 958-962.
24. Quanru, G.; Guitang, P.; Zheng, L.; Chen, Z.; Fisher, R.D.; Sun, Z.; Ou, C.; Dong, H.; Wang, X.; Li, S. The Eastern Himalayan syntaxis: major tectonic domains, ophiolitic mélanges and geologic evolution. Journal of Asian Earth Sciences **2006**, 27, 265-285.
25. Zhang, Z.; Dong, X.; Santosh, M.; Liu, F.; Wang, W.; Yiu, F.; He, Z.; Shen, K. Petrology and geochronology of the Namche Barwa Complex in the eastern Himalayan syntaxis, Tibet: constraints on the origin and evolution of the north-eastern margin of the Indian Craton. Gondwana Research **2012**, 21, 123-137.
26. Ding, L.; Zhong, D. Metamorphic characteristics and geotectonic implications of the high-pressure granulites from Namjagbarwa, eastern Tibet. Science in China Series D: Earth Sciences **1999**, 42, 491-505.
27. Yin, A.; Harrison, T.M. Geologic evolution of the Himalayan-Tibetan orogen. Annual review of earth and planetary sciences **2000**, 28, 211-280.
28. Qi, X.; Li, H.; Li, T.; Cai, Z.; Yu, C. U-Pb dating for garnet-rich granite veins in high-pressure granulites from the Namche Barwa complex, eastern syntaxis of the Himalayas, and the relationship with exhumation. Acta Petrologica Sinica **2010**, 26, 975-984.
29. Heng, L.; Jin, Z.; Pan, G.; Sun, Z.; Geng, Q. A Geological Comparison between the Eastern and Western Himalayan Syntaxes. Earth Science **2004**, 29, 269-277.
30. Geng, Q.; Pan, G.; Liu, Y.; Zheng, L. The preliminary study of the ophiolitic melanges along the Yarlung Zangbo Grand Canyon, Xizang. Sedimentary Geology and Tethyan Geology **2000**, 20, 28-43.
31. Peng, S.; Ding, Y.; Liu, W.; Zhi, L.I. 1 km monthly temperature and precipitation dataset for China from 1901 to 2017. Earth System Science Data **2019**, 11, 1931–1946.
32. Scherler, D.; Bookhagen, B.; Strecker, M.R. Correction to "Tectonic control on 10Be-derived erosion rates in the Garhwal Himalaya, India". Journal of Geophysical Research: Earth Surface **2014**, 119(4), 960-960.
33. Schmidt, K.M.; Montgomery, D.R. Limits to relief. Science **1995**, 270, 617-620.
34. Feng, Z.; Li, W.; Li, P.; Xiao, C. Relief degree of land surface and its geographical meanings in the Qinghai-Tibet Plateau, China. Acta Geogr. Sin **2020**, 75, 1359-1372.
35. Strahler, A.N. Hypsometric (area-altitude) analysis of erosional topography. Geological society of America bulletin **1952**, 63(11), 1117-1142.
36. Snyder, N.P.; Whipple, K.X.; Tucker, G.E.; Merritts, D. J. Landscape response to tectonic forcing: Digital elevation model analysis of stream profiles in the Mendocino triple junction region, northern California. Geological Society of America Bulletin **2000**, 112(8), 1250-1263.
37. Schwanghart, W.; Scherler, D. TopoToolbox 2–MATLAB-based software for topographic analysis and modeling in Earth surface sciences. Earth Surface Dynamics **2014**, 2(1), 1-7.
38. Perron, J.T.; Royden, L. An integral approach to bedrock river profile analysis. Earth surface processes and landforms **2013**, 38, 570-576.
39. Willett, S.D.; McCoy, S.W.; Perron, J.T.; Goren, L.; Chen, C.-Y. Dynamic reorganization of river basins. Science **2014**, 343, 1248765.
40. Giachetta, E.; Willett, S.D. Effects of river capture and sediment flux on the evolution of plateaus: insights from numerical modeling and river profile analysis in the upper Blue Nile catchment. Journal of Geophysical Research: Earth Surface **2018**, 123, 1187-1217.
41. Royden, L.; Taylor Perron, J. Solutions of the stream power equation and application to the evolution of river longitudinal profiles. Journal of Geophysical Research: Earth Surface **2013**, 118, 497-518.

42. Whipple, K.X.; DiBiase, R.A.; Ouimet, W.B.; Forte, A.M. Preservation or piracy: Diagnosing low-relief, high-elevation surface formation mechanisms. Geology **2017**, 45, 91-94.
43. Yang, R.; Willett, S.D.; Goren, L. In situ low-relief landscape formation as a result of river network disruption. Nature **2015**, 520, 526-529.
44. Jaiswara, N.K.; Pandey, P.; Pandey, A.K. Mio-Pliocene piracy, relict landscape and drainage reorganization in the Namcha Barwa syntaxis zone of eastern Himalaya. Scientific reports **2019**, 9, 17585.
45. Kirby, E.; Whipple, K.X. Expression of active tectonics in erosional landscapes. Journal of Structural Geology **2012**, 44, 54-75.
46. Zeitler, P.; Malloy, M.; Kutney, M.; Idleman, B.; Liu, Y.; Kidd, W.; Booth, A. TI: Geochronological Evidence for the Tectonic and Topographic Evolution of SE Tibet. **2006**.
47. Malloy, M. Rapid erosion at the Tsangpo knickpoint and exhumation of southeastern Tibet. Lehigh University Bethlehem, PA, USA, 2004.
48. Yu, X.; Ji, J.; Gong, J.; Sun, D.; Qing, J.; Wang, L.; Zhong, D.; Zhang, Z. Evidences of rapid erosion driven by climate in the Yarlung Zangbo (Tsangpo) Great Canyon, the eastern Himalayan syntaxis. Chinese Science Bulletin **2011**, 56, 1123-1130.
49. Gong, J.; Ji, J.; Zhou, J.; Tu, J.; Sun, D.; Zhong, D.; Han, B. Late Miocene thermal evolution of the eastern Himalayan syntaxis as constrained by biotite 40Ar/39Ar thermochronology. The Journal of Geology **2015**, 123, 369-384.
50. Tu, J.-Y.; Ji, J.-Q.; Sun, D.-X.; Gong, J.-F.; Zhong, D.-L.; Han, B.-F. Thermal structure, rock exhumation, and glacial erosion of the Namche Barwa Peak, constraints from thermochronological data. Journal of Asian Earth Sciences **2015**, 105, 223-233.
51. van der Beek, P.; Schildgen, T.F. age2exhume–a MATLAB/Python script to calculate steady-state vertical exhumation rates from thermochronometric ages and application to the Himalaya. Geochronology **2023**, 5, 35-49.
52. Evans, S.G.; Delaney, K.B. Characterization of the 2000 Yigong Zangbo River (Tibet) landslide dam and impoundment by remote sensing. In Natural and artificial rockslide dams; Springer: 2010; pp. 543-559.
53. Chong, X.; Xiwei, X.; Bengang, Z.; Lingling, S. Probability of coseismic landslides: A new generation of earthquake-triggered landslide hazard model. Journal Of Engineering Geology **2019**, 27(5), 1122-1130.
54. DiBiase, R.A.; Whipple, K.X.; Heimsath, A.M.; Ouimet, W.B. Landscape form and millennial erosion rates in the San Gabriel Mountains, CA. Earth and Planetary Science Letters **2010**, 289, 134-144.
55. Goren, L.; Willett, S.D.; Herman, F.; Braun, J. Coupled numerical–analytical approach to landscape evolution modeling. Earth Surface Processes & Landforms **2014**, 39, 522-545.
56. Burg, J.P.; Davy, P.; Nievergelt, P.; Oberli, F.; Seward, D.; Diao, Z.; Meier, M. Exhumation during crustal folding in the Namche-Barwa syntaxis. Terra Nova **1997**, 9(2), 53-56.
57. Seward, D.; Burg, J. P. Growth of the Namche Barwa Syntaxis and associated evolution of the Tsangpo Gorge: Constraints from structural and thermochronological data. Tectonophysics **2008**, 451(1-4), 282-289.
58. Enkelmann, E.; Ehlers, T.A.; Zeitler, P.K.; Hallet, B. Denudation of the Namche Barwa antiform, eastern Himalaya. Earth and Planetary Science Letters **2011**, 307(3-4), 323-333.
59. Govin, G., Najman, Y., Dupont-Nivet, G., Millar, I., Van Der Beek, P., Huyghe, P., O'sullivan, P., Mark, C., Vögeli, N. The tectonics and paleo-drainage of the easternmost Himalaya (Arunachal Pradesh, India) recorded in the Siwalik rocks of the foreland basin. American Journal of Science **2018**, 318, 764-798.
60. Burg, J.P.; Podladchikov, Y. Lithospheric scale folding: numerical modelling and application to the Himalayan syntaxes. International Journal of Earth Sciences **1999**, 88, 190-200.
61. Bendick, R.; Ehlers, T; A. Extreme localized exhumation at syntaxes initiated by subduction geometry. Geophysical Research Letters **2014**, 41(16), 5861-5867.
62. Whipp Jr D.M.; Beaumont, C.; Braun, J. Feeding the "aneurysm": Orogen-parallel mass transport into Nanga Parbat and the western Himalayan syntaxis. Journal of Geophysical Research: Solid Earth **2014**, 119(6), 5077-5096.
63. Gupta, T.D.; Riguzzi, F.; Dasgupta, S.; Mukhopadhyay, B.; Roy, S.; Sharma, S. Kinematics and strain rates of the Eastern Himalayan Syntaxis from new GPS campaigns in Northeast India. Tectonophysics **2015**, 655, 15-26.

 doi:10.20944/preprints202402.0554.v1